九州大学学術情報リポジトリ
Kyushu University Institutional Repository

Electrochemical Characterization, Structural Evolution, and Thermal Stability of LiVOPO_4 over Multiple Lithium Intercalations

Nojima, Akinobu
Institute for Materials Chemistry and Engineering, Kyushu University

Sano, Atsushi
Energy Devices Business Group, TDK Corporatio

Kitamura, Hiroki
Energy Devices Business Group, TDK Corporatio

Okada, Shigeto
Institute for Materials Chemistry and Engineering, Kyushu University

https://doi.org/10.5109/2547346

出版情報：Evergreen. 6 (4), pp.267-274, 2019-12. Transdisciplinary Research and Education Center for Green Technologies, Kyushu University
バージョン：
権利関係：Creative Commons Attribution-NonCommercial 4.0 International

KYUSHU UNIVERSITY

Electrochemical Characterization, Structural Evolution, and Thermal Stability of $LiVOPO_4$ over Multiple Lithium Intercalations

Akinobu Nojima[1, 2], Atsushi Sano[2], Hiroki Kitamura[2], Shigeto Okada[1]

[1]Institute for Materials Chemistry and Engineering, Kyushu University, Japan

[2]Energy Devices Business Group, TDK Corporation, Japan

*Author to whom correspondence should be addressed:
E-mail: anojima@jp.tdk.com

(Received November 5, 2019; Revised December 5, 2019; accepted December 6, 2019).

Abstract: α_1-$LiVOPO_4$, β-$LiVOPO_4$, and α-$LiVOPO_4$ are known as multiple lithium intercalation cathode materials. They were characterized by means of half-cell performance, *operando* X-ray diffraction (XRD), X-ray absorption spectroscopy (XAS), and differential scanning calorimetry (DSC). The *operando* XRD revealed differences in crystal structure evolution during charging/ discharging among the three crystal phases. Although the charge/discharge profiles and the crystal structure evolution behaviors were the same among the three crystal phases in the range of 3.5 - 4.5 V, the profiles and behaviors differed completely in the range of 1.0 - 3.5 V. The thermal stability of each phase of $LiVOPO_4$ is similar to that of $LiFePO_4$ in the fully charged state from the results of the DSC profiles.

Keywords: evergreen; Lithium ion battery, Cathode material, $LiVOPO_4$

1. Introduction

Lithium ion secondary batteries (LIBs) have high energy density, so they are used in a wide range of applications such as smartphones, notebook PCs, and electric vehicles. Battery performance is related to cathode material properties. For example, layered rock salt metal oxide materials such as $LiCoO_2$ have high energy density, making them suitable for smartphones and notebook PCs, but they could not be expected to have long cycle lives or a high degree of safety because of their low crystal structure stability. Since Co is a limited natural resource, an alternative cathode material to $LiCoO_2$ is required. Polyanion cathode materials such as $LiFePO_4$ have high thermal stability and high crystal structure stability because PO_4 has strong covalent bonds that prevent oxygen release[1-4] and achieved long cycle lives [5-6], but its energy density is lower than that of $LiCoO_2$, so it is suitable for nonmobile devices that require long cycle lives and a high degree of safety, such as energy storage systems.

Multi-electron phosphate and oxyphosphate materials such as $Li_3V_2(PO_4)_3$ [7-8] and $LiVOPO_4$ [9-17] have attracted attention as alternatives to $LiFePO_4$ due to their higher energy densities. Rui *et al.* reported the characteristics of $Li_3V_2(PO_4)_3$ as an anode and showed that Li intercalated stepwise between 2.0 V and 1.6 V and was about 130 mAh /g; however, its energy density is too low for it to be useful as an anode active material [18]. Moreover, $Li_3V_2(PO_4)_3$ could not be extracted last lithium, and the capacity related to the V^{3+}/V^{4+} couples [19]. On the other hand, $LiVOPO_4$ has three types of crystal structure: α_1-$LiVOPO_4$ (tetragonal phase) [9-11, 20-21], β-$LiVOPO_4$ (orthorhombic phase) [12-14, 22-25], and α-$LiVOPO_4$ (triclinic phase; some reports described the third type as ε-$LiVOPO_4$) [15-17, 26-29]. Good electrochemical performance was found by the use of both the V^{3+}/V^{4+} and V^{4+}/V^{5+} redox couples. The crystal structure evolution from $LiVOPO_4$ to Li_2VOPO_4 in relation to α_1-$LiVOPO_4$ [9], β-$LiVOPO_4$ [12-13], and α-$LiVOPO_4$ [15-16] has been studied, but the discharge voltages were 1.5 V, so it is hard to discuss the possibility of _valence of vanadium becoming less than a trivalent state and generates larger capacity. Although $LiVOPO_4$ is expected to have high thermal stability because it consists of PO_4, no report has actually evaluated this.

In our previous study, we succeeded in producing three phases of lithium vanadium oxyphosphate (α_1-$LiVOPO_4$, β-$LiVOPO_4$, α-$LiVOPO_4$) from the same precursor that was synthesized by the hydro-thermal method [30]. In this study, we used these $LiVOPO_4$ to reveal the relationship between electrochemical properties and crystal structure evolution in the low-voltage region up to 1.0 V using *operando* XRD and XAFS. We also discussed the thermal stability of $LiVOPO_4$

2. Experimental

Three phases of $LiVOPO_4$ were prepared by a hydrothermal method and subsequent sintering process as previously reported [30]. The prepared $LiVOPO_4$ was mixed with acetylene black at a weight ratio of 92:8, and ball milling was used to downsize the $LiVOPO_4$ particles and to carbon coat the surface. The crystal structure of each phase was confirmed using powder X-ray diffractometer (Ultima IV, Rigaku) with Cu Kα radiation (λ = 0.15418 nm).

The electrochemical characterization was carried out with Al laminate-type cells assembled in a dry room in which the dew point was -40°C. Electrodes were fabricated by casting the slurry, which was made from the downsized and carbon-coated $LiVOPO_4$ and PVDF (polyvinylidene fluoride) at a weight ratio 92:8 in NMP (N-Methylpyrrolidone). The active material was around 6 mg/cm^2 on Al foil. The half-cell type of Al laminate cells were used, consisting of the $LiVOPO_4$ electrode as a cathode, Li metal on Cu as an anode, and a separator (2400, Celgard). As an electrolyte, 1 M of $LiPF_6$ in a solution of ethylene carbonate (EC) and diethyl carbonate (DEC; volume ratio of EC:DEC=3:7) was used. Charge/discharge testing was performed by a battery charge/discharge system (SM-8, Hokuto Denko) at room temperature.

The crystal structure evolution of $LiVOPO_4$ during charging and discharging was measured by *operando* X-ray diffraction (XRD) in transmission geometry (Empyrean, Panalytical), using the same configuration of half-cells described above. The charge/discharge rate was C/10 at the voltage range of 4.8 - 1.0 V for the first charge/discharge and for the charge to 3.9 V. XRD patterns were collected every hour. The scan rate of a scan was 360 s, and the 2θ step size was 0.026° in the 2θ range of 10-36°.

The vanadium valence of $LiVOPO_4$ in discharge states was analyzed from the V-K edge X-ray absorption near-edge structure (XANES). *Ex situ* X-ray absorption spectroscopy (XAS) measurements for V-K edge absorption were performed at beamline BL05S1 at the Aichi Synchrotron Radiation Center. The measured electrode samples were extracted from disassembled cells, which had been discharged at target voltage and resealed by an Al laminate in a glove box. The XAS data were collected in quick-scan mode. XANES data were normalized by using Athena developed by Ravel and Newville [31]. Energy was calibrated by using XANES of vanadium thin foil.

The thermal stability of $LiVOPO_4$ was evaluated by a differential scanning calorimetry (DSC, DSC6220, Hitachi) method at a heating rate of 5°C/min up to 400°C. Cells at the target voltage were disassembled in a glove box and the electrodes were washed with DEC. Subsequently, punch out with 3 mm of diameter from the electrode. Three sheets of punched-out samples were packed into stainless steel DSC capsules with 4.5 mg of electrolyte and then hermetically sealed.

3. Results and Discussion

Figure 1 shows the first and second charge/discharge curves of α_1-, β-, and α-$LiVOPO_4$ in the voltage range of 1.0 - 4.5 V at a rate of 0.05 C (1C = 1.07 mA/cm^2). The profiles were the same at the first charge, but the discharge profiles and second charge profiles clearly differed among the three phases. The first charge and discharge capacities of α_1-$LiVOPO_4$ were 123 mAh/g and 288 mAh/g, respectively. The characteristics of the α_1-$LiVOPO_4$ charge/discharge curve correspond to those of previous reports [9-10]. Although the first charge capacity of our α_1-$LiVOPO_4$ was lower than those previously published values, the discharge capacity accorded with the discharge capacities considering different cutoff voltages. Discharge capacity from 3.0 - 1.0 V was 165 mAh/g, even though the theoretical capacity of the reaction ($LiVOPO_4$ (V^{4+}) ↔ Li_2VOPO_4 (V^{3+})) is 159 mAh/g. Therefore, it could be expected that the valence of vanadium was decreased to below V^{3+}. On the other hand, charging from 1.0 V requires high voltage to deintercalate Li, which is associated with overpotential [11]. Therefore, the second charge capacity from 3.0 - 4.5 V was larger than the first. The first charge and discharge capacities of β-$LiVOPO_4$ were 139 mAh/g and 354 mAh/g, respectively. Three plateau regions appeared in the discharge curve at 3.9, 2.0, and 1.1 V. The first (V^{5+}/V^{4+}) and second (V^{4+}/V^{3+}) plateaus corresponded to previous reports [12-14, 17]. The discharge capacity from 3.0 - 1.0 V was 215 mAh/g. Apparently this is larger than the theoretical capacity, so the valence of vanadium should be decreased to below V^{3+} or the structure change from β-$LiVOPO_4$ to Li_3PO_4 occurred as Ren *et al.* reported [14]; if the valence of vanadium decreased, the reaction at the third plateau could be considered to be a V^{3+}/V^{2+} redox couple. The capacity of the second plateau region was 134 mAh/g, which almost matched the first charge capacity. Unlike the case with α_1-$LiVOPO_4$, the V^{4+}/V^{3+} discharge did not achieve theoretical capacity. On the other hand, the voltage profile of the second charge was slightly out of shape. The first charge capacity of α-$LiVOPO_4$ was 99 mAh/g, but the discharge capacity from 4.5 - 1.0 V was 257 mAh/g and the capacity of 3.0 - 1.0V was 158 mAh/g. That is, the theoretical capacity could be achieved in the low-voltage region. This indicates that the lithium intercalate ability differs between high- and low-voltage regions. Furthermore, the voltage profile is relatively the same for charging and discharging. Three distinct plateaus appeared in the range of 2.5 - 1.9 V. This reaction, in which the valence of vanadium is tetravalent and trivalent, has been discussed in detail [12-13, 15-16]. Hence the reaction of V^{3+}/V^{2+} cannot be expected in the region of 1.0 - 4.5 V.

The cycle characteristics were evaluated under the rate of C/20 (first and second cycles) and the C/10 condition. The cycle characteristics of the 2^{nd}, 10^{th}, 20^{th}, and 30^{th} charge/discharge curves are shown in Fig. 2 and indicate that the cycle characteristics were not stable. The capacity in the range of 3.0 - 4.5 V was almost constant, but the

capacity of the low-voltage region decreased as the cycle number increased. This was attributed to the disappearance of V^{3+}/V^{4+} reactions. The capacity retention of α-$LiVOPO_4$ was good compared to the other phases but slightly worse than in previous reports [16-17].

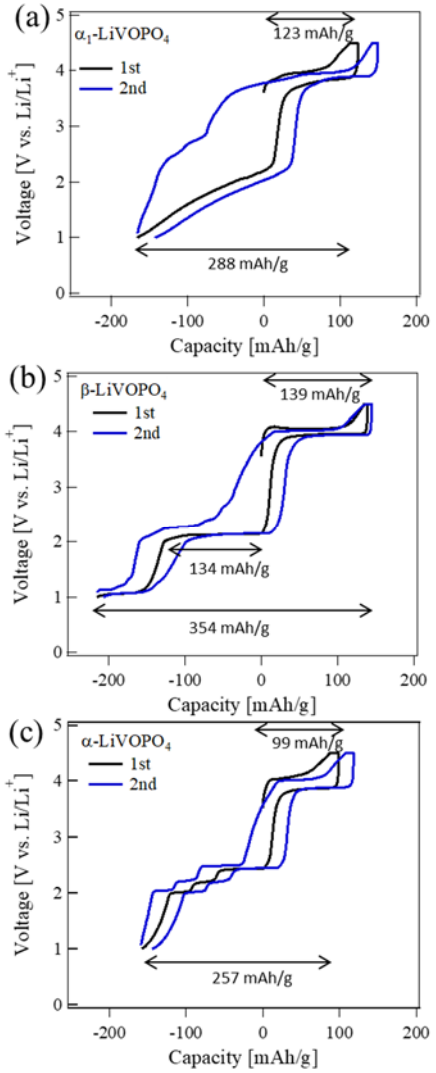

Fig. 1: First and second charge/discharge curves of α_1-$LiVOPO_4$ (a), β-$LiVOPO_4$ (b), and α-$LiVOPO_4$ (c) in the range of 4.5–1.0 V at the rate of C/20.

In order to understand the phase evolution of each $LiVOPO_4$ during charge/discharge, *operando* XRD was performed on an X-ray diffractometer equipped with Cu-Kα1 radiation in transmission geometry, together with the charge/discharge data. The charging and discharging rate was C/10 in the voltage range of 3.5 - 4.8 V for the first charge, 4.8 - 1.0 V for the first discharge, and 1.0 - 3.9 V for the second charge. Every pattern was recorded in the 2θ range of 10-36° every hour, corresponding to x = 0.1 in Li_xVOPO_4. The results are shown in Fig. 3 (α1-$LiVOPO_4$), Fig. 4 (β-$LiVOPO_4$), and Fig. 5 (α-$LiVOPO_4$). Since there was not enough active material on the electrode, sufficient signal intensity could not be detected. We therefore discuss the whether the crystal structure evolution is two-phase or solid-solution behavior, based on changes in the main peak. If it was two-phase behavior, diffraction peaks from two kinds of crystal phase would be found simultaneously and no diffraction peak shifts would be found. If it was solid-solution behavior, on the other hand, a diffraction peak shift would be found.

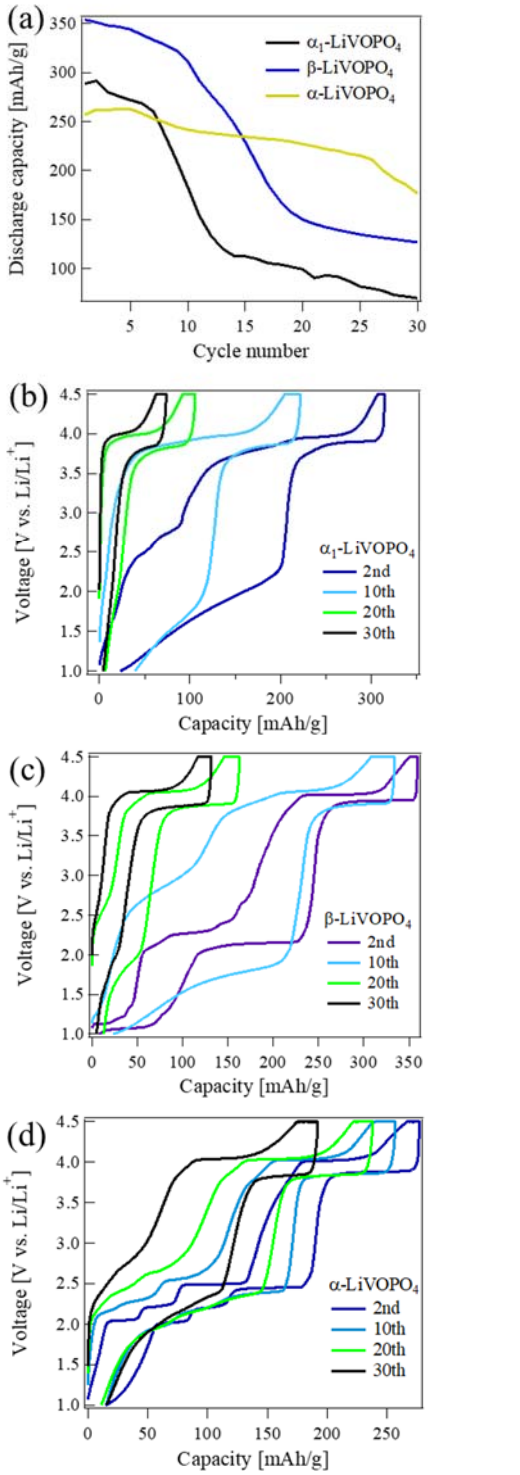

Fig. 2: Cycle characteristics of α_1-$LiVOPO_4$, β-$LiVOPO_4$, and α-$LiVOPO_4$ in the 4.5–1.0 V range at the rates of C/20 (first and second cycles) and C/10 (a). The 2nd, 10th, 20th, and 30th charge/discharge curves of α_1-$LiVOPO_4$ (b), β-$LiVOPO_4$ (c), and α-$LiVOPO_4$ (d).

Variations in the diffraction peaks of α_1-$LiVOPO_4$

correspond to the results of *ex situ* XRD reported by G. He *et al.* [9]. The final diffraction pattern fully corresponded to the initial diffraction pattern. This suggests that the reaction is highly reversible even though the crystal structure changes dynamically. In the discharge from 4.8 - 1.0 V, the diffraction peak of α_1-$LiVOPO_4$ decreases, that of α_1-Li_2VOPO_4 increases, and that of α_1-$LiVOPO_4$ continues to appear distinctly up to 1.5 V. The state of structural change is clearly different between charging and discharging. In discharging, the diffraction peaks of α_1-$LiVOPO_4$ and α_1-Li_2VOPO_4 can be distinguished as two-phase behavior. However, in charging from 1.0 V as the voltage increased, the shape of the peak collapsed, the full width at half maximum widened and gradually shifted to the high-angle side, indicating solid-solution behavior. It can be considered that the difference between Li^+ intercalation and deintercalation behaviors is associated with the difference in charge/discharge profiles in the low-voltage region. This supports two-phase behavior in low-voltage discharge as G. He *et al.* reported [9]. However, it is solid-solution behavior in charging at low voltage.

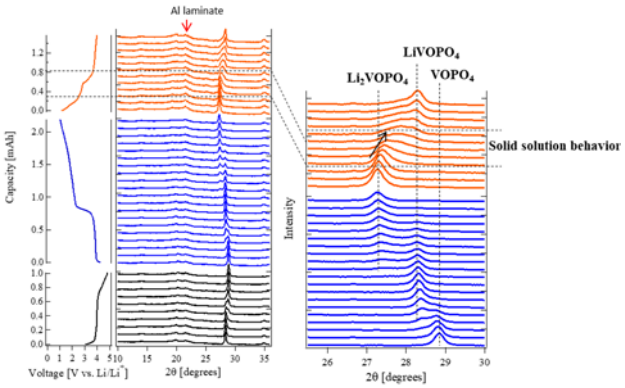

Fig. 3: *Operando* XRD patterns of α_1-$LiVOPO_4$ with charge/discharge profiles at C/10 up to 4.8 V (left). An enlarged view of the 25.5–30° region of the first discharge and second charge. The dotted lines indicate the characteristic peak positions of the crystal phases.

Figure 4 shows the results of *operand* XRD for β-$LiVOPO_4$. There are drastic changes in the XRD patterns as the amount of lithium changes. In the first charge, a peak shift was not found and only diffraction peaks from each phases increase and decrease. This indicates two-phase behavior. In the first discharge, as the black arrows indicate, a diffraction peak shift is found in the latter half of the second plateau (2.1 V). The peak shift started after the $LiVOPO_4$ peaks disappeared. After the peak shift (corresponding to the end of the second plateau), the peak location was not changed but the intensity started to decrease, and this diffraction peak disappeared at the third plateau. M. M. Ren *et al.* revealed that the crystal structure of discharging β-$LiVOPO_4$ at 0.01 V changed to Li_2O, V and Li_3PO_4 [14]. However, we could not find such components, but two new weak peaks appeared at the 2θ region of 26-27°. Due to low crystallinity, we did not know how to attribute the peaks. At least it could be said that, before Li_2VOPO_4 decomposes to Li_2O, V and Li_3PO_4 at 0.01 V, another crystal phases would exist. In the second charge, although an unknown peak was found at the lower plateau region as indicated by the black dashed arrow, the positions and behaviors of the other diffraction peaks agreed with those in discharging. Thus, unlike the case with α_1-$LiVOPO_4$, the phase transition behaviors were the same in charging as in discharging. Therefore, in the charge/discharge curve, the plateau of low voltage appears at the same voltage during charging and discharging.

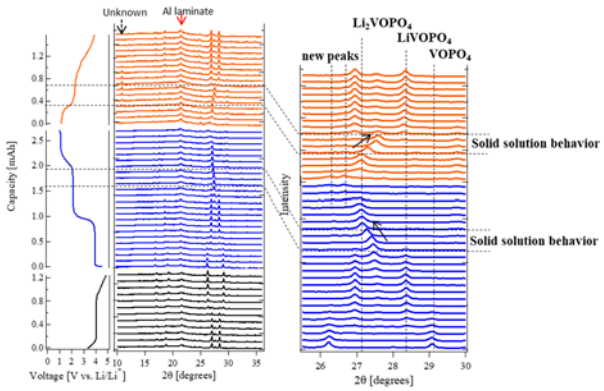

Fig. 4: *Operando* XRD patterns of β-$LiVOPO_4$ with charge/discharge profiles at C/10 up to 4.8 V (left). An enlarged view of the 25.5–30° region of the first discharge and second charge. The dotted lines indicate the characteristic peak positions of the crystal phases.

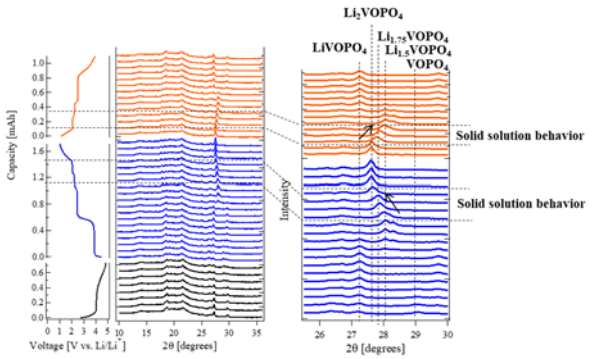

Fig. 5: *Operando* XRD patterns of α-$LiVOPO_4$ with charge/discharge profiles at C/10 up to 4.8 V (left). Enlarged view of the 25.5–30° region of the first discharge and second charge. The dotted lines indicate the characteristic peak positions of the crystal phases.

The results of *operando* XRD for α-$LiVOPO_4$ are shown in Fig. 5. The capacity of our α-$LiVOPO_4$ was half of theoretical capacity, so that the diffraction peaks of both $VOPO_4$ and α-$LiVOPO_4$ appeared at 4.8 V. Considering the results of our previous study, lithium would perhaps not be deintercalate from large particles, [30] and the diffraction peak of α-$LiVOPO_4$ would be from large particles. As shown in Fig. 1 (c), three peculiar plateaus appeared in the low-voltage region. As shown in Fig. 5, the plateau of 2.4 V ($LiVOPO_4 \leftrightarrow Li_{1.5}VOPO_4$) indicates two-phase behavior, and the plateaus of 2.2 V ($Li_{1.5}VOPO_4 \leftrightarrow Li_{1.75}VOPO_4$) and 2.0 V ($Li_{1.75}VOPO_4 \leftrightarrow$

Li_2VOPO_4) indicate solid-solution behavior because peak shifts occurred. These results agreed with that of previous report [15]. In charging from 1.0 V, the crystal structure evolution was the same as in discharging. Therefore, α-$LiVOPO_4$ also exhibits plateaus at the same voltage in charging and discharging. Interestingly, because diffraction peaks of α-$LiVOPO_4$ clearly disappeared, unlike the case in 4.8 V charging, large particles also contribute to low-voltage charging/discharging.

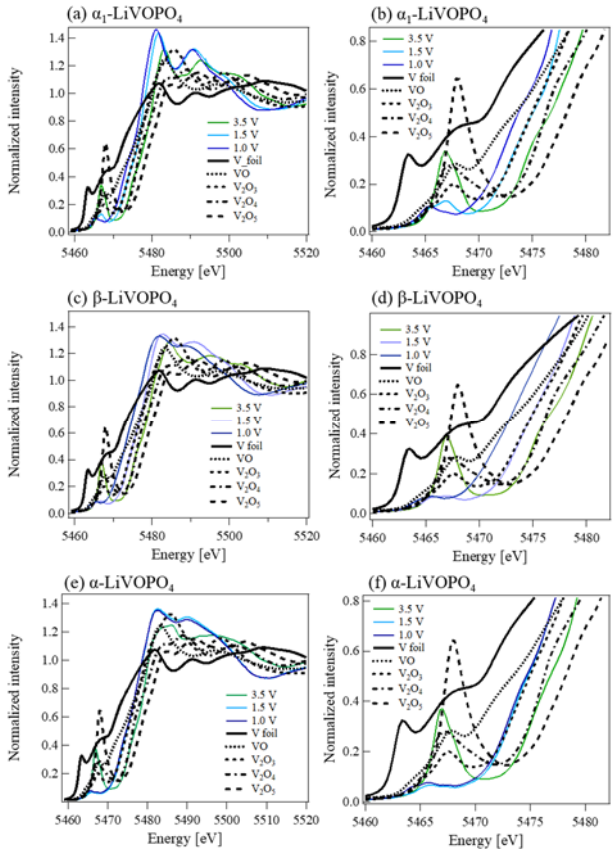

Fig. 6: Normalized V K-edge XANES spectra of α1-$LiVOPO_4$ (a), (b), β-$LiVOPO_4$ (c), (d), and α-$LiVOPO_4$ (e), (f) at various states of OCV comparisons of various vanadium oxides and vanadium metal. (b), (d), and (f) are enlarged views of the pre-edge peaks.

As mentioned above, the discharge capacities from 3.5 - 1.0 V of α1-$LiVOPO_4$ and β-$LiVOPO_4$ were larger than the theoretical capacity of $LiVOPO_4$ (V^{4+}) ↔ Li_2VOPO_4 (V^{3+}). On the other hand, α-$LiVOPO_4$ exhibited the theoretical capacity even though the charge capacity from 3.5 - 4.5 V was 99 mAh/g. To explain this capacity from the viewpoint of charge compensation, information on the valence of vanadium at low voltage is needed. *Ex situ* XAFS was performed to investigate the valence of vanadium in the low-voltage region and the results were compared with those of various vanadium oxides and vanadium metal as a standard valence. The results of the normalized XANES spectra are shown in Fig. 6. The pre-edge shape varied and energy shifts were seen, according to OCV changes. The pre-edge peak is due to the 1s → 3d tradition, which is possible because of the O 2p and V 3d/4p hybrid orbit. The large pre-edge peak is attributable to the distortion of the VO_6 octahedra due to V=O [12-13]. The pre-edge peak decreased as OCV decreased. This change trend of β-$LiVOPO_4$ and α-$LiVOPO_4$ agreed with previous reports [12-13]. From the results of the XANES absorption edge shift, the valences of vanadium for α1-$LiVOPO_4$ and β-$LiVOPO_4$ at 1.5 V and for α-$LiVOPO_4$ at 1.5 V and 1.0 V should be V^{+3} because they corresponded to the absorption edge of V_2O_3. Although it is difficult to determine the valences of vanadium at 1.0 V of α1-$LiVOPO_4$ and β-$LiVOPO_4$, it can be said that it is sufficiently smaller than at least trivalent. This study revealed the vanadium valence behavior of α1-$LiVOPO_4$ in the low-voltage region using XAFS. G. He *et al.* reported the crystal structure of α1-Li_2VOPO_4 using neutron and X-ray diffraction with Rietveld refinement. V-O bonding of α1-Li_2VOPO_4 was longer than α1-$LiVOPO_4$, and the summary of bond valance sums of vanadium for the vanadium coordination environment in α1-Li_2VOPO_4 was trivalent. [9] From our XANES results, the trivalent of vanadium was OCV at 1.5 V, and α1-$LiVOPO_4$ must finish changing to α1-Li_2VOPO_4 at 1.5 V in discharging. This is supported by our *operando* XRD as shown in Fig. 3, where the crystal structure finished changing around 1.5 V. Additional lithium insertion from 1.5 - 1.0 V suggests that the framework of the crystal structure is not changing; rather, only the valence of vanadium changes.

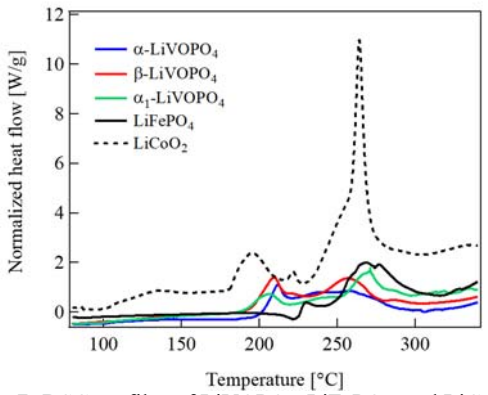

Fig. 7: DSC profiles of $LiVOPO_4$, $LiFePO_4$, and $LiCoO_2$ with electrolyte at a heating rate of 5°C/min after 4.5 V charge for $LiVOPO_4$ and $LiCoO_2$, and 3.8 V for $LiFePO_4$.

The thermal stability of $LiVOPO_4$ was investigated using DSC. Figure 7 shows DSC profiles of α1-$LiVOPO_4$, β-$LiVOPO_4$, α-$LiVOPO_4$, and $LiCoO_2$ at 4.5 V charge and $LiFePO_4$ at 3.8 V charge. The DSC profiles of all $LiVOPO_4$ had the same shape and were similar to $LiFePO_4$. All PO_4 tetrahedral corners of $LiVOPO_4$ are shared with VO_6 octahedra, which is different from the case with $LiFePO_4$. $LiFePO_4$ shares one edge of PO_4 tetrahedra with FeO_6 octahedra. However, the difference in crystal structures is not related to thermal stability. Since both $LiVOPO_4$ and $LiFePO_4$ are composed of highly thermostable PO_4, there is no oxygen release, so

there is no clear difference in DSC profiles. Figure 8 shows the DSC profiles of $LiVOPO_4$ at 4.5 V charging and 1.0 V discharging. These profiles differ. It is difficult to discuss a strictly quantitative comparison of the total exothermic reaction enthalpy because the baseline and temperature range for calculating total exothermic enthalpy for each datum cannot always be constant. The exothermic enthalpy values are shown in Fig. 8 as reference values. The exothermic reaction enthalpy of $LiVOPO_4$ is small enough compared with $LiCoO_2$. Although α_1-, β-, and α-$LiVOPO_4$ discharged down to 1.0 V have different crystal structures and amounts of Li, they all showed a similar slight exothermic reaction around 90°C. Although we could not determine the reason for the exothermic reaction at 1.0 V of the profile around 90°C, the exothermic reaction enthalpy is around 190 J/g at most, which is considered too low to reduce thermal stability. The high thermal stability of $LiVOPO_4$ is maintained even in the low-voltage region.

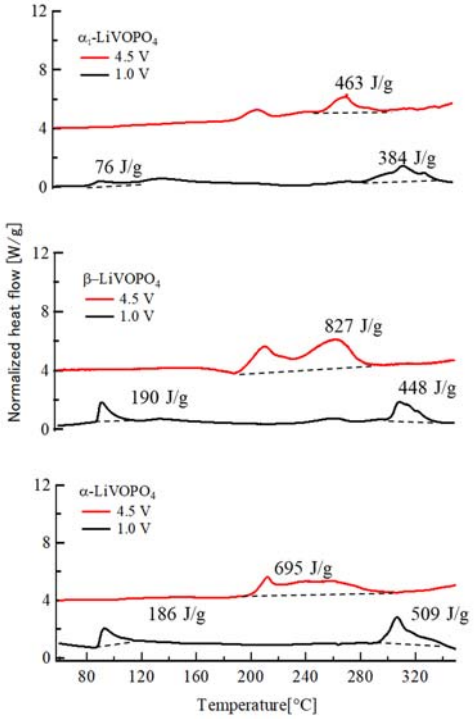

Fig. 8: DSC profiles of $LiVOPO_4$ at 4.5 V charging and 1.0 V discharging with electrolyte at a heating rate of 5°C/min.

4. Conclusions

α_1-, β-, and α-$LiVOPO_4$ have been synthesized from the same precursor, and controlled subsequent sintering temperature. The capacities in the ranges of 3.5 - 4.5 V and 3.5 - 1.0 V differed. The capacity of the high-voltage region is influenced by the particle size, although the capacity of the low-voltage region was close to the theoretical capacity. Moreover, α_1- and β-$LiVOPO_4$ exhibited beyond theoretical capacity in discharging to 1.0 V due to the decrease in the vanadium valence to below V^{3+}. This was supported by *ex situ* XANES analysis. *Operando* XRD determined whether the crystal structure evolution was solid-solution behavior or two-phase behavior during charging/discharging, and the difference in the charge/discharge profiles of α_1-$LiVOPO_4$ was associated with crystal structure evolution. The thermal stability of $LiVOPO_4$ was demonstrated by DSC for the first time. The DSC profiles of $LiVOPO_4$ in the charging state were similar to that of $LiFePO_4$ and the total exothermic enthalpy were smaller than that of $LiCoO_2$. Although the root cause could not be identified, the DSC profile of $LiVOPO_4$ at 1.0 V appeared as an exothermic reaction around 90°C. However, it was not so large, and the total exothermic enthalpy from 80 - 350°C was the same as that at 4.5 V charging. Since α_1-, β-, and α-$LiVOPO_4$ have high energy densities and high thermal stabilities, we conclude that they can be expected to serve not only as a next-generation polyanion cathode materials to replace $LiFePO_4$ but also as an anode materials with high thermal stability.

Acknowledgements

The author(s) received no financial support for the research, authorship, and/or publication of this article.

References

1) A.K. Padhi, K.S. Nanjundaswamy, and J.B. Goodenough,"Phospho-olivines as Positive-Electrode Materials for Rechargeable Lithium Batteries," *J. Electrochem. Soc.*, **144** (*4*) 1188–1194 (1997). doi: 10.1149/1.1837571.
2) A.K. Padhi, K.S. Nanjundaswamy, C. Masquelier, S. Okada, and J.B. Goodenough, "Effect of Structure on the Fe^{3+} / Fe^{2+} Redox Couple in Iron Phosphates," *J. Electrochem. Soc.*, **144** (*5*) 1609–1613 (1997). doi: 10.1149/1.1837649.
3) A. Yamada and S.C. Chung, "Crystal Chemistry of the Olivine-Type $Li(Mn_yFe_{1-y})PO_4$ and $(Mn_yFe_{1-y})PO_4$ as Possible 4 V Cathode Materials for Lithium Batteries," *J. Electrochem. Soc.*, **148** (*8*) A960–A967 (2001). doi: 10.1149/1.1385377.
4) K. Amine, H. Yasuda, and M. Yamachi, "Olivine $LiCoPO_4$ as 4.8 V Electrode Material for Lithium Batteries," *Electrochem. Solid-State Letters*, **3** (*4*) 178–179 (2000). doi: 10.1149/1.1390994.
5) M. Takahashi, H. Ohtsuka, K. Akuto, and Y. Sakurai, "Confirmation of Long-Term Cyclability and High Thermal Stability of $LiFePO_4$ in Prismatic Lithium-Ion Cells," *J. Electrochem. Soc.*, **152** (*5*) A899–A904 (2005). doi: 10.1149/1.1874693.
6) E.R. Dyartanti, I.N. Widiasa, A. Purwanto, and H. Susanto, "Nanocomposite Polymer Electrolytes in PVDF/ZnO Membranes Modified with PVP for use in $LiFePO_4$ Batteries," *Evergreen*, **5** (*2*) 19–25 (2018). doi: 10.5109/1936213.
7) M.Y. Saidi, J. Barker, H. Huang, J.L. Swoyer, and G. Adamson, "Performance characteristics of lithium vanadium phosphate as a cathode material for

lithium-ion batteries," *J. Power Sources*, **119-121** 266–272 (2003). doi: 10.1016/S0378-7753(03)00245-3.

8) H. Huang, S.C. Yin, T. Kerr, N. Taylor, and L.F. Nazar, "Nanostructured Composites: A High Capacity, Fast Rate $Li_3V_2(PO_4)_3$/Carbon Cathode for Rechargeable Lithium Batteries, " *Adv. Mater*., **14** (*21*) 1525–1528 (2002). doi: 10.1002/1521-4095(20021104)14:21<1525::AID-ADMA1525>3.0.CO;2-3.
9) G. He, C.A. Bridges, and A. Manthiram, "Crystal Chemistry of Electrochemically and Chemically Lithiated Layered α_I-$LiVOPO_4$," *Chem. Mater.*, **27** (*19*) 6699–6707 (2015). doi: 10.1021/acs.chemmater.5b02609.
10) N.F. Quackenbush, L. Wangoh, D.O. Scanlon, R. Zhang, Y. Chung, Z. Chen, B. Wen, Y. Lin, J.C. Woicik, N.A. Chernova, S.P. Ong, M.S. Whittingham, and L.F.J. Piper, "Interfacial Effects in ε-Li_xVOPO_4 and Evolution of the Electronic Structure," *Chem. Mater.*, **27** (*24*) 8211–8219 (2015). dio: 10.1021/acs.chemmater.5b02145.
11) Z. Chen, Q. Chen, L. Chen, R. Zhang, H. Zhou, N.A. Chernova and M.S. Whittingham, "Electrochemical Behavior of Nanostructured ε-$VOPO_4$ over Two Redox Plateaus," *J. Electrochem. Soc.*, **160** (*10*) A1777–A1780 (2013). doi: 10.1149/2.064310jes.
12) K.L. Harrison, C.A. Bridges, C.U. Segre, C.D. Varnado Jr., D. Applestone, C.W. Bielawski, M.P. Paranthaman, and A. Manthiram, "Chemical and Electrochemical Lithiation of $LiVOPO_4$ Cathodes for Lithium-Ion Batteries," *Chem. Mater.*, **26** (*12*) 3849–3861 (2014). doi: 10.1021/cm501588j.
13) C.J. Allen, Q. Jia, C.N. Chinnasamy, S. Mukerjee, and K.M. Abraham, "Synthesis, Structure and Electrochemistry of Lithium Vanadium Phosphate Cathode Materials," *J. Electrochem. Soc.*, **158** (*12*) A1250–A1259 (2011). doi: 10.1149/2.003112jes.
14) M.M. Ren, Z. Zhou, and X.P. Gao, "$LiVOPO_4$ as an anode material for lithium ion batteries," *J. Appl. Electrochem.*, **40** 209–213 (2010). doi: 10.1007/s10800-009-9958-3.
15) M. Bianchini, J.M. Ateba-Mba, P. Dagault, E. Bogdan, D. Carlier, E. Suard, C. Masquelierade, and L. Croguennec, "Multiple phases in the ε-VPO_4O–$LiVPO_4O$–Li_2VPO_4O system: a combined solid state electrochemistry and diffraction structural study," *J. Mater. Chem. A*, **2** 10182–10192 (2014). doi: 10.1039/C4TA01518E.
16) Y.C. Lin, B. Wen, K.M. Wiaderek, S. Sallis, H. Liu, S.H. Lapidus, O.J. Borkiericz, N.F. Quachenbush, N. A. Chernova, K. Karki, F. Omenya, P.J. Chupas, L.F. J. Piper, M.S. Whittingham, K.W. Chapman, and S.P. Ong, "Thermodynamics, Kinetics and Structural Evolution of ε-$LiVOPO_4$ over Multiple Lithium Intercalation," *Chem. Mater.*, **28** (*6*) 1794–1805 (2016). doi: 10.1021/acs.chemmater.5b04880.
17) H. Zhou, Y. Shi, F. Xin, F. Omenya, and M.S. Whittingham, "ε- and β-$LiVOPO_4$: Phase Transformation and Electrochemistry," *Appl. Mater. Interfaces*, **9** (*34*) 28537–28541 (2017). doi: 10.1021/acsami.7b07895.
18) X.H. Rui, N. Yesibolati, and C.H. Chen, "$Li_3V_2(PO_4)_3$/C composite as an intercalation-type anode material for lithium-ion batteries," *J. Power Sources*, **199** (*4*) 2279–2282 (2011). doi: 10.1016/j.jpowsour.2010.09.024.
19) G. Hautier, A. Jian, S.P. Ong, B. Kang, C. Moore, R. Doe, and G. Ceber, "Phosphates as Lithium-Ion Battery Cathodes: An Evaluation Based on High-Throughput ab Initio Calculations," *Chem. Mater.*, **23** (15) 3495–3508 (2011). doi: 0.1021/cm200949v.
20) N. Dupre, G. Wallez, J. Gaubicher, and M. Quarton, "Phase transition induced by lithium insertion in α_I- and α_{II}-$VOPO_4$," *J. Solid State Chem.*, **117** (*8*) 2896–2902 (2004). doi: 10.1016/j.jssc.2004.04.006.
21) A.S. Hameed, M. Nagarathinam, M.V. Reddy, B.V.R. Chowdan, and J.J. Vittal, "Synthesis and electrochemical studies of layer-structured metastable α_I-$LiVOPO_4$," *J. Mater. Chem.*, **22** 7206–7213 (2012). doi: 10.1039/C2JM00062H.
22) J. Barker, M.Y. Sadi, and J.L. Swoyer, "Electrochemical Properties of Beta- $LiVOPO_4$ Prepared by Carbothermal Reduction," *J. Electrochem. Soc*., **151** (*6*) A796–A800 (2004). doi: 10.1149/1.1723494.
.23) B.M. Azmi, T. Ishihara, H. Nishiguchi, and Y. Takita, "$LiVOPO_4$ as a new cathode materials for Li-ion rechargeable battery," *J. Power Sources*, **146** (*1-2*) 525–528 (2005). doi: 10.1016/j.jpowsour.2005.03.101.
24) M.M. Ren, Z. Zhou, L.W. Su, and X.P. Gao, "$LiVOPO_4$: A cathode material for 4 V lithium ion batteries," *J. Power Sources*, **189** (*1*) 786–789 (2009). doi: 10.1016/j.jpowsour.2008.07.092.
25) L. Wang, L. Yang, L. Gong, X. Jiang, K. Yuan, and Z. Hu, "Synthesis of $LiVOPO_4$ for cathode materials by coordination and microwave sintering," *Electrochim. Acta*, **56** (*20*) 6906–6911 (2011). doi: 10.1016/j.electacta.2011.06.028.
26) Y. Yang, H. Fang, J. Zheng, L. Li, G. Li, and G. Yan, "Towards the understanding of poor electrochemical activity of triclinic $LiVOPO_4$: Experimental characterization and theoretical investigations," *Solid State Sci.*, **10** (*10*) 1292–1298 (2008). doi: 10.1016/j.solidstatesciences.2008.01.028.
27) A. Tang, J. Shen, Y. Hu, G. Xu, D. He, Q. Yi, and R. Peng, "Electrochemical Performance of α-$LiVOPO_4$/Carbon Composite Material Synthesized by Sol–Gel Method," *J. Electrochem. Soc.*, **161** (*1*) A10–A13 (2014). doi: 10.1149/2.005401jes.
28) Z. Liu, Z. Su, and H. Tian, "Synthesis and electrochemical properties of α-$LiVOPO_4$ as cathode material for lithium-ion batteries," *Ceram. Int*., **44** (*8*)

9372–9376 (2018). doi: 10.1016/j.ceramint.2018.02.151.

29) K. Saravanan, H.S. Lee, M. Kuezma, J.J. Vittal, and P. Balaya, "Hollow α-$LiVOPO_4$ sphere cathodes for high energy Li-ion battery application," *J. Mater. Chem.*, **21** (*27*) 10042–10050 (2011). doi: 10.1039/C0JM04428H.
30) A. Nojima, A. Sano, S. Fujita, K. Ohtsuki, and S. Okada, "Evaluation of α_1-$LiVOPO_4$, β-$LiVOPO_4$, and α-$LiVOPO_4$ Synthesized from a Same Precursor by Hydrothermal Method," *J. Electrochem. Soc*., **166** (*15*) A3731–A3738 (2019). doi: 10.1149/2.0691915jes.
31) B. Ravel and M. Newville, "ATHENA, ARTEMIS, HEPHAESTUS: data analysis for X-ray absorption spectroscopy using IFEFFIT," *J. Synchrotron Radiat*., **12** 537–541 (2005). doi: 10.1107/S0909049505012719.